*Mathematika* 61 (2015) 444–456 © 2014 University College London
doi:10.1112/S0025579314000321

# DYNAMIC MULTI-STRUCTURE IN MODELLING A TRANSITION FLEXURAL WAVE

ALEXANDER B. MOVCHAN, MICHELE BRUN,
LEONID I. SLEPYAN AND GIAN F. GIACCU

*Dedicated to Professor Vladimir Maz'ya on the occasion of his 75th birthday*

*Abstract.* This paper presents a model of a 1D–1D dynamic multi-structure, supporting propagation of a transition wave. It is used to explain the recent phenomenon of the collapse of the San Saba bridge. An analytical model is supplied with illustrative numerical simulations.

§1. *Introduction.* This paper addresses a lower-dimensional dynamic model of a 1D–1D multi-structure supporting a transition wave.

The notion of multi-structures was introduced in Ciarlet [5, 6] and LeDret [8]. The asymptotic analysis of fields in multi-structures and related analysis of eigenvalue problems was published in Kozlov *et al* [7]. This also included a vector case of the Lamé system for structures including 3D bodies and thin rods. Panasenko [10] includes multi-scale analysis of lattice-like multi-structures and, in particular, applications in modelling of elastic rods connected at junction points.

In the present paper, we consider a mathematical model of gravity driven failure of a long bridge supported by periodically distributed pillars. The multi-structure approximation involves a governing equation of a flexural beam with periodically distributed pointed sources whose intensities are linked to a Floquet wave propagating along such a structure. It is appropriate to refer to Brun *et al* [2, 3] where the notion of structured waveguides was successfully used in the modelling of real engineering structures, such as bridges, in challenging projects that required a design of so-called passive mass dampers that control undesired swaying of the structure.

Furthermore, the model is advanced by incorporating a semi-infinite moving fault, and consequently a transition wave. Formally, it is also similar in many ways to models of fracture of discrete lattice systems as in Slepyan [11] and Mishuris *et al* [9], and the analysis is reduced to the study of a functional equation of the Wiener–Hopf type. There is an apparent link with the Floquet waves mentioned earlier, as well as quasi-periodic Green's functions [1], as they are incorporated into the kernel function of the Wiener–Hopf equation mentioned.

Received 23 April 2014, published online 5 December 2014.
MSC (2010): 35Q15, 45E10, 35Q74 (primary).

https://doi.org/10.1112/S0025579314000321 Published online by Cambridge University Press

The structure of the paper is as follows. Section 2 introduces the quasi-periodic Green's function for a flexural system, and the dispersion equation for a periodically supported flexural system is presented in a simple form. Dispersion equations are readily available, and the relevant analysis is given in the text to emphasize the connection between the Floquet waves in an infinite periodic system and vibrations of a finite elongated structure.

Section 3 introduces a semi-infinite moving fault in connection with the model of a failing bridge. The model describes a real event – the spectacular collapse of San Saba railway bridge in Central Texas, which was the subject of media attention across the world. In §4 we give an equivalent formulation written for a functional equation of the Wiener–Hopf type for a transition wave in a semi-discrete flexural system. Section 5 presents a continuous homogenized model leading to a closed-form explicit solution. Finally, §6 deals with the evaluation of parameters of the transition wave and, in particular, with the evaluation of the speed of the steady-state propagation.

§2. *Quasi-periodic Green's functions and dispersion of flexural waves.* Green's kernels provide model solutions for equations with point sources representing external forces. We consider a multi-structure that includes an infinite elastic waveguide supported by a periodic array of "springs" or "pillars", whose input can be brought into the model as a point force. Assuming that these springs are linear, and the waveguide itself is a flexural beam, one would need the classical Green's function $g(x, x_0; \omega)$ that satisfies the equations

$$D\frac{\partial^4 g(x, x_0; \omega)}{\partial x^4} - \rho A\, \omega^2 g(x, x_0; \omega) + \delta(x - x_0) = 0, \tag{1}$$

where $\omega$ is the radian frequency, $D$ the bending stiffness (assumed constant), $\rho$ the density, $A$ the cross-sectional area and $\delta$ the Dirac-delta function. It has the form

$$g(x, x_0; \omega) = \frac{1}{4D\alpha^3}(\mathrm{e}^{\alpha|x-x_0|} + \mathrm{i}\mathrm{e}^{-\mathrm{i}\alpha|x-x_0|}), \tag{2}$$

where

$$\alpha = (\rho A\omega^2/D)^{1/4}. \tag{3}$$

By distributing the supporting pillars periodically, with a period $a$, and assuming that the elastic wave is characterized by a frequency $\omega$ and a wave number $k$, we would need a quasi-periodic Green's function defined by

$$G(x, x_0; \omega, k) = \sum_{n=-\infty}^{+\infty} g(x, x_0 + na; \omega)\mathrm{e}^{\mathrm{i}kna}, \tag{4}$$

which simplifies, in the case $x = x_0 = 0$, to

$$\begin{aligned} G_0(\omega, k) &= G(0, 0; \omega, k) \\ &= \frac{1}{4D\alpha^3}\left[1 + \frac{\cos(ka) - \mathrm{e}^{-\alpha a}}{\cosh(\alpha a) - \cos(ka)} - \frac{\sin(\alpha a)}{\cos(\alpha a) - \cos(ka)}\right]. \end{aligned} \tag{5}$$

https://doi.org/10.1112/S0025579314000321 Published online by Cambridge University Press

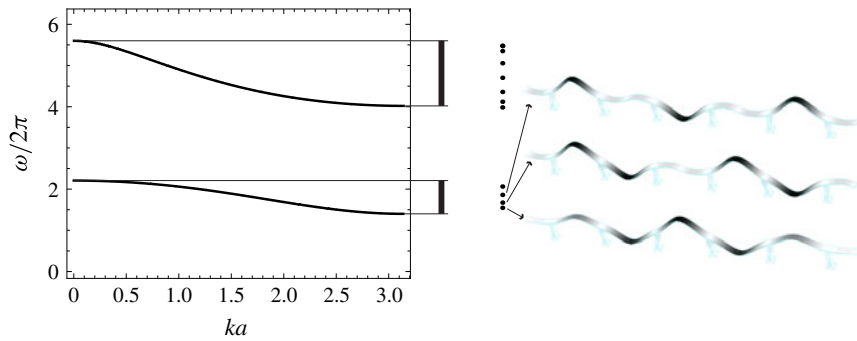



Figure 1: Flexural vibrations of an elastically supported bridge model. Dispersion properties relating the radian frequency $\omega$ and the wave number $k$ are given for a typical automotive bridge: Young's Modulus $E = 34\,209$ MPa, mass density per unit volume $\rho = 2400$ kg m$^{-3}$, span length $a = 90$ m and stiffness of the vertical support $\gamma_z = 500$ MPa m. The black dots are the eigenfrequency of a six-span structure. Three corresponding eigenmodes are also given.

The junction condition at a point $x = 0$, where the linear elastic pillar supports the main waveguide, is

$$G_0(\omega, k) = \frac{1}{\gamma}, \tag{6}$$

where $\gamma$ represents the stiffness for the supporting element. Equation (6) is the dispersion equation for Floquet–Bloch waves in the periodically supported flexural waveguide.

One of the important features shown on the dispersion diagram in Figure 1 is the presence of the so-called band gaps, where the above dispersion equation does not have real solutions. Namely, for a given frequency with such a band gap, the solution $k$ of the dispersion equation is complex, and the corresponding wave is evanescent. We also note that a continuous beam without periodically distributed forces (applied at the junction points between the main deck of the bridge and the supporting pillars) would not show band gaps (except for a possible stop band adjacent to the origin for beams on a Winkler foundation).

The information about the frequencies corresponding to the pass bands is important, as it provides bounds for eigenfrequencies of the finite long structure. Also shown in Figure 1 are black dots corresponding to eigenfrequencies of a six-span bridge, and they are all projected into the interval, which corresponds to a pass band of an infinite periodic structure. An illustrative computation of the flexural deformation for some of the eigenmodes is also shown in Figure 1.

Figure 2 shows that the dispersion curves in question are sandwiched between the curves representing solutions of the equation

$$\alpha = \pm k + \frac{2\pi n}{a}, \tag{7}$$

where $\alpha$ is proportional to the square root of the frequency as in (3). We note that these values correspond to singularities of the lattice sums, and they also correspond to flexural waves propagating along the homogeneous unconstrained

https://doi.org/10.1112/S0025579314000321 Published online by Cambridge University Press

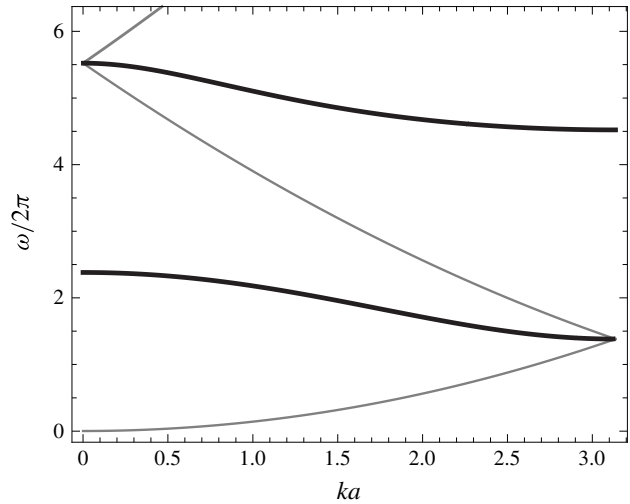



Figure 2: Dispersion properties of the periodically supported beam. Dispersion curves are given in black, grey lines correspond to singularities of the lattice sum, which also satisfy equation (7).

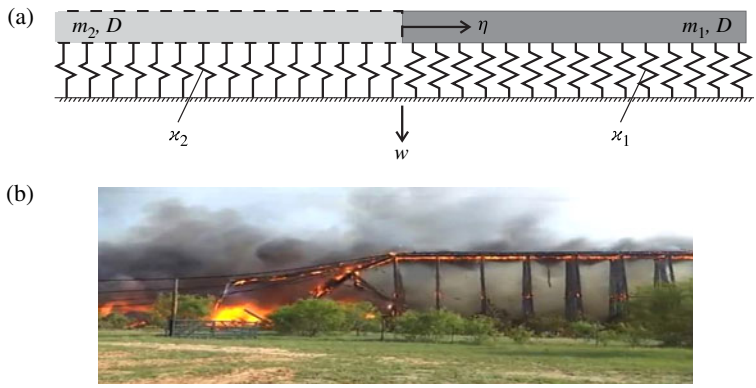



Figure 3: (a) Supported beam models. Undamaged and damaged parts are indicated with subscripts 1 and 2, respectively. The beam has mass density $m_{1,2} = m^0_{1,2} + M_{1,2}/a$ and bending stiffness $D$; the foundation has stiffness per unit length $\varkappa_{1,2} = \varkappa^0_{1,2}/a$. (b) Snapshot of the collapse of the San Saba bridge.

flexural beam. In particular, the positions of the intersection points in Figure 2 are independent of $\gamma$.

§3. *A semi-infinite fault.* Examples of semi-infinite faults include semi-infinite cracks in unbounded solids, and semi-infinite stamps moving on a surface of an elastic half-space or a half-plane. And in all such cases, the solution of the corresponding problem is not smooth near the edge of the fault.

We consider a non-standard configuration of a "discrete fault" for a flexural wave, for whom the elastic supports on the left of the origin are different from those on the right of the origin. An illustration of such an unusual fault is shown in Figure 3(b). Furthermore, we refer to Figure 3(a) which depicts failure of a

https://doi.org/10.1112/S0025579314000321 Published online by Cambridge University Press

Table 1: Notation for the stiffness of the supporting pillars, mass at the junction points and distributed mass within the flexural beams ahead and behind the transition point $\eta = 0$.

| | $\varkappa^0$ | $M$ | $m^0$ |
|---|---|---|---|
| $\eta > 0$ | $\varkappa_1^0$ | $M_1$ | $m_1^0$ |
| $\eta < 0$ | $\varkappa_2^0 < \varkappa_1^0$ | $M_2$ | $m_2^0$ |

bridge. The spectacular collapse of the San Saba bridge in Texas in 2013 was accompanied by a transition wave that represented a discrete fault, linked to change of stiffness of elastic pillars as the bridge collapsed. It is shown here that our model explains this phenomenon of dynamic failure.

Discrete faults are well-defined in the framework of functional equations of the Wiener–Hopf type as in [**11**], with the assumption that the problem is referred to a moving system of coordinates, where the constant speed is also called the propagation speed of the fault.

3.1. *Governing equations describing the motion of a semi-discrete system with a moving fault.* The equations of motion for the flexural displacement $w$ are

$$\begin{gathered} D\frac{\partial^4 w(x,\eta)}{\partial x^4} + m_1^0 \frac{\partial^2 w(x,\eta)}{\partial t^2} = m_1^0 g \quad (x \neq an); \\ M_1 \frac{\partial^2 w(\eta)}{\partial t^2} + \varkappa_1^0 w(\eta) = M_1 g + \mathcal{V}^+(\eta) - \mathcal{V}^-(\eta), \\ \mathcal{M}^+(\eta) = \mathcal{M}^-(\eta) \quad (x = an). \end{gathered} \tag{8}$$

The coefficients have the following physical meaning: $D$ is the bending stiffness, $m_1^0$ is the beam mass† per unit length and $g$ is the gravity acceleration; $\mathcal{V}^{\pm}(\eta)$ and $\mathcal{M}^{\pm}(\eta)$ are the transverse force and the bending moment. The superscript $^{\pm}$ indicates that these quantities are evaluated on the right or on the left of the junction point $x = na$. Here, it is also assumed that an elastic beam is placed on elastic supports at $x = na$, $a > 0$, $n = 0, \pm 1, \ldots$.

Furthermore, we consider a fault, with the transition point $\eta = 0$, so that the notation in Table 1 is introduced.

The steady-state regime is considered in the sense that the displacement $w$ at $x = na$ is a function of $\eta = na - vt$.

It is convenient to use the following length and time units:

$$\xi = (D/\varkappa_1)^{1/4}, \qquad \tau = \sqrt{m_1/\varkappa_1},$$

with $\varkappa_1 = \varkappa_1^0/a$, and the mass density unit $m_1 = m_1^0 + M_1/a$. In these terms, the

† In the text above, the notation $\rho$ was used for the mass density; hence here $m_1^0 = \rho A$, where $A$ is the cross-sectional area of the beam.

https://doi.org/10.1112/S0025579314000321 Published online by Cambridge University Press

normalized quantities denoted by tilde are

$$
\begin{gathered}
(x, a, \eta, w) = \xi(\tilde{x}, \tilde{a}, \tilde{\eta}, \tilde{w}), \qquad M_{1,2} = m_1 a \tilde{M}_{1,2}, \\
(t, \omega^{-1}) = \tau(\tilde{t}, \tilde{\omega}^{-1}), \qquad v = (\xi/\tau)\tilde{v}, \qquad g = (\xi/\tau^2)\tilde{g}, \\
\mathcal{V}(x, \eta) = -D\frac{\partial^3 w(x, \eta)}{\partial x^3} = \frac{D}{\xi^2}\tilde{\mathcal{V}}(\tilde{x}, \tilde{\eta}), \qquad \tilde{\mathcal{V}}(\tilde{x}, \tilde{\eta}) = -\frac{\partial^3 \tilde{w}(\tilde{x}, \tilde{\eta})}{\partial \tilde{x}^3}, \\
\mathcal{M}(x, \eta) = D\frac{\partial^2 w(x, \eta)}{\partial x^2} = \frac{D}{\xi}\tilde{\mathcal{M}}(\tilde{x}, \tilde{\eta}), \qquad \tilde{\mathcal{M}}(\tilde{x}, \tilde{\eta}) = \frac{\partial^2 \tilde{w}(\tilde{x}, \tilde{\eta})}{\partial \tilde{x}^2}.
\end{gathered} \tag{9}
$$

The normalized equations of motion (8) become

$$
\frac{\partial^4 \tilde{w}(\tilde{x}, \tilde{\eta})}{\partial \tilde{x}^4} + \frac{m_1^0}{m_1}\frac{\partial^2 \tilde{w}(\tilde{x}, \tilde{\eta})}{\partial \tilde{t}^2} = \frac{m_1^0}{m_1}\tilde{g} \quad (x \neq an); \tag{10}
$$

$$
\begin{gathered}
\tilde{M}_1\frac{\partial^2 \tilde{w}(\tilde{\eta})}{\partial \tilde{t}^2} + \tilde{w}(\eta) = \tilde{M}_1\tilde{g} + \frac{\tilde{\mathcal{V}}^+(\tilde{\eta}) - \tilde{\mathcal{V}}^-(\tilde{\eta})}{\tilde{a}}, \\
\tilde{\mathcal{M}}^+(\tilde{\eta}) = \tilde{\mathcal{M}}^-(\tilde{\eta}) \quad (x = an).
\end{gathered} \tag{11}
$$

Recall that in the damaged region, $\eta < 0$, the values $\varkappa_1^0$, $M_1$, $m_1^0$ are replaced by $\varkappa_2^0 < \varkappa_1^0$, $M_2$ and $m_2^0$. For this case, equation (10) and the first equation in (11) take the form

$$
\frac{\partial^4 \tilde{w}(\tilde{x}, \tilde{\eta})}{\partial \tilde{x}^4} + \frac{m_2^0}{m_1}\frac{\partial^2 \tilde{w}(\tilde{x}, \tilde{\eta})}{\partial \tilde{t}^2} = \frac{m_2^0}{m_1}\tilde{g} \quad (x \neq an); \tag{12}
$$

$$
\tilde{M}_2\frac{\partial^2 \tilde{w}(\tilde{\eta})}{\partial \tilde{t}^2} + \frac{\varkappa_2}{\varkappa_1}\tilde{w}(\tilde{\eta}) = \tilde{M}_2\tilde{g} + \frac{\tilde{\mathcal{V}}^+(\tilde{\eta}) - \tilde{\mathcal{V}}^-(\tilde{\eta})}{\tilde{a}} \quad (x = an). \tag{13}
$$

We use the substitutions

$$
\tilde{w}(x, \eta) = g + \frac{m_1^0}{24\, m_1}(x - an)^2(x - a(n+1))^2 g + \bar{w}(x, \eta), \tag{14}
$$

and

$$
\tilde{\mathcal{V}}^{\pm}(\eta) = \pm\frac{m_1^0}{m_1}\frac{g\, a}{2} + \bar{\mathcal{V}}^{\pm}(\eta), \qquad \tilde{\mathcal{M}}^{\pm}(\eta) = \frac{m_1^0}{m_1}\frac{g\, a^2}{12} + \bar{\mathcal{M}}^{\pm}(\eta) \tag{15}
$$

to obtain that for $\eta > 0$

$$
\begin{gathered}
x \neq an: \quad \frac{\partial^4 \bar{w}(x, \eta)}{\partial x^4} + \frac{m_1^0}{m_1}\frac{\partial^2 \bar{w}(x, \eta)}{\partial t^2} = 0; \\
x = an: \quad M_1\frac{\partial^2 \bar{w}(\eta)}{\partial t^2} + \bar{w}(\eta) = \frac{\bar{\mathcal{V}}^+(\eta) - \bar{\mathcal{V}}^-(\eta)}{a}, \\
\bar{\mathcal{M}}^+(\eta) = \bar{\mathcal{M}}^-(\eta),
\end{gathered} \tag{16}
$$

https://doi.org/10.1112/S0025579314000321 Published online by Cambridge University Press

and for $\eta < 0$

$$
\begin{aligned}
x \neq an: \quad & \frac{\partial^4 \bar{w}(x,\eta)}{\partial x^4} + \frac{m_2^0}{m_1}\frac{\partial^2 \bar{w}(x,\eta)}{\partial t^2} = \frac{m_2^0 - m_1^0}{m_1} g; \\
x = an: \quad & M_2 \frac{\partial^2 \bar{w}(\eta)}{\partial t^2} + \frac{\varkappa_2}{\varkappa_1}\bar{w}(\eta) = \frac{\bar{\mathcal{V}}^+(\eta) - \bar{\mathcal{V}}^-(\eta)}{a} + C, \\
& \bar{\mathcal{M}}^+(\eta) = \bar{\mathcal{M}}^-(\eta), \\
& C = g(1 - \varkappa_2/\varkappa_1 + M_2 - M_1).
\end{aligned}
\tag{17}
$$

In the following text, the symbols "bar" and "tilde" are omitted for convenience of notation. We also restrict our attention to the case where the damage is concentrated at the pillars positioned at $x = na$, and $m_1^0 = m_2^0 = m^0$.

3.2. *Intensities of sources at junction points of the multi-structure.* The elastic flexural bridge supported by periodically allocated pillars is referred to as a 1D–1D multi-structure in the asymptotic approximation that uses a one-dimensional model for an upper deck of the bridge and one-dimensional model for axial deformations of the supporting pillars. In turn, the junction points are identified as the points of intersection between a segment representing a pillar and the line representing the elastic bridge.

Consider neighboring cross-sections placed at the elastic support points, say, at $x = 0$ and at $x = a$. The displacement of the beam between these cross-sections satisfies the equation

$$
\frac{\partial^4 w(x,\eta)}{\partial x^4} + v^2 \frac{m^0}{m_1}\frac{\partial^2 w(x,\eta)}{\partial \eta^2} = 0. \tag{18}
$$

In terms of the Fourier transform on $\eta$ with parameter $k$ we have

$$
\frac{\partial^4 w^F(x,k)}{\partial x^4} - v^2 k^2 \frac{m^0}{m_1} w^F(x,k) = 0 \quad \text{with } v^2 k^2 = -\lim_{\varepsilon \to +0} (\varepsilon + \mathrm{i}vk)^2. \tag{19}
$$

To compute the dynamic stiffness coefficients we make use of an auxiliary solution corresponding to the boundary conditions

$$
w^F(0,k) = (w^F(0,k))' = 0, \qquad w^F(a,k) = w_0, \qquad (w^F(a,k))' = \phi_0. \tag{20}
$$

The Fourier transforms of the normalized transverse shear force $\mathcal{V} = -w'''$ and the normalized bending moment $\mathcal{M} = w''$ are as follows:

$$
\begin{aligned}
\begin{pmatrix} \mathcal{V}^F(0,k) \\ \mathcal{V}^F(a,k) \end{pmatrix} &= \begin{bmatrix} \mathcal{V}_{w0} & \mathcal{V}_{\phi 0} \\ \mathcal{V}_{wa} & \mathcal{V}_{\phi a} \end{bmatrix} \begin{pmatrix} w_0 \\ \phi_0 \end{pmatrix}, \\
\begin{pmatrix} \mathcal{M}^F(0,k) \\ \mathcal{M}^F(a,k) \end{pmatrix} &= \begin{bmatrix} \mathcal{M}_{w0} & \mathcal{M}_{\phi 0} \\ \mathcal{M}_{wa} & \mathcal{M}_{\phi a} \end{bmatrix} \begin{pmatrix} w_0 \\ \phi_0 \end{pmatrix},
\end{aligned}
\tag{21}
$$

https://doi.org/10.1112/S0025579314000321 Published online by Cambridge University Press

with

$$\mathcal{V}_{w0} = \frac{\lambda^3(\sinh\lambda a + \sin\lambda a)}{1-\cosh\lambda a\cos\lambda a}, \quad \mathcal{V}_{\phi 0} = -\frac{\lambda^2(\cosh\lambda a - \cos\lambda a)}{1-\cosh\lambda a\cos\lambda a},$$
$$\mathcal{V}_{wa} = \frac{\lambda^3(\cosh\lambda a\sin\lambda a + \sinh\lambda a\cos\lambda a)}{1-\cosh\lambda a\cos\lambda a}, \quad \mathcal{V}_{\phi a} = -\frac{\lambda^2\sinh\lambda a\sin\lambda a}{1-\cosh\lambda a\cos\lambda a},$$
$$\mathcal{M}_{w0} = \frac{\lambda^2(\cosh\lambda a - \cos\lambda a)}{1-\cosh\lambda a\cos\lambda a}, \quad \mathcal{M}_{\phi 0} = -\frac{\lambda(\sinh\lambda a - \sin\lambda a)}{1-\cosh\lambda a\cos\lambda a},$$
$$\mathcal{M}_{wa} = -\frac{\lambda^2\sinh\lambda a\sin\lambda a}{1-\cosh\lambda a\cos\lambda a}, \quad \mathcal{M}_{\phi a} = \frac{\lambda(\cosh\lambda a\sin\lambda a - \sinh\lambda a\cos\lambda a)}{1-\cosh\lambda a\cos\lambda a}, \tag{22}$$

where $\lambda = (m^0/m_1)^{1/4}\sqrt{kv - \mathrm{i}0}$.

§4. *Wiener–Hopf functional equation.* Following the Fourier transforms and using (21) and (22), (16) and (17) can be written in terms of the functions

$$w_+(k) = \int_0^\infty w(\eta)\mathrm{e}^{\mathrm{i}k\eta}\,d\eta, \qquad w_-(k) = \int_{-\infty}^0 w(\eta)\mathrm{e}^{\mathrm{i}k\eta}\,d\eta, \tag{23}$$

which satisfy the functional equation

$$\begin{aligned}
&L_1(k)w_+(k) + L_2(k)w_-(k)\\
&\quad = \frac{C}{0+\mathrm{i}k} = \frac{C(L_1(k)-L_2(k))}{(0+\mathrm{i}k)[1-\varkappa_2/\varkappa_1 + (M_1-M_2)(0+\mathrm{i}kv)^2]},\\
&L_1(k) = 1 + M_1(0+\mathrm{i}kv)^2\\
&\qquad + \frac{2}{a}\left[(\mathcal{V}_{wa} - \mathcal{V}_{w0}\cos ka) + \frac{\mathcal{V}_{\phi 0}\mathcal{M}_{w0}\sin^2 ka}{\mathcal{M}_{\phi a} - \mathcal{M}_{\phi 0}\cos ka}\right],\\
&L_2(k) = \frac{\varkappa_2}{\varkappa_1} + M_2(0+\mathrm{i}kv)^2\\
&\qquad + \frac{2}{a}\left[(\mathcal{V}_{wa} - \mathcal{V}_{w0}\cos ka) + \frac{\mathcal{V}_{\phi 0}\mathcal{M}_{w0}\sin^2 ka}{\mathcal{M}_{\phi a} - \mathcal{M}_{\phi 0}\cos ka}\right].
\end{aligned} \tag{24}$$

Thus, the Wiener–Hopf equation takes the form

$$\begin{aligned}
&L_0(k)w_+(k) + w_-(k)\\
&\quad = \frac{C}{(0+\mathrm{i}k)[1-\varkappa_2/\varkappa_1 + (M_1-M_2)(0+\mathrm{i}kv)^2]}\left[\frac{L_1(k)}{L_2(k)} - 1\right].
\end{aligned} \tag{25}$$

We note that after the substitution $v = \omega/k$ into $L_j$ $(j = 1, 2)$ in (24), equations $L_1 = 0$ and $L_2 = 0$ become the dispersion relations for the undamaged and damaged structures, respectively, describing the Bloch–Floquet wave propagation within the two types of periodic systems. They correspond to the dispersion equation (6) of §2, which was written in terms of the quasi-periodic Green's function (5).

https://doi.org/10.1112/S0025579314000321 Published online by Cambridge University Press

4.1. *Factorization.* The non-dimensional beam equation after the Fourier transform on $\eta$ becomes

$$\frac{\partial^4 w^F(x,k)}{\partial x^4} - v^2 k^2 w^F(x,k) = 0, \tag{26}$$

and we use notation

$$L(k) = \frac{M_2}{M_1}\frac{L_1(k)}{L_2(k)} \to 1 \quad (k \to \pm\infty). \tag{27}$$

We also note that its index is zero, i.e.

$$\operatorname{Ind} L(k) = \frac{1}{2\pi}[\operatorname{Arg} L(\infty) - \operatorname{Arg} L(-\infty)] = 0. \tag{28}$$

The factorization is as follows:

$$\begin{aligned} L(k) &= \lim_{\Im k \to 0} L_+(k) L_-(k), \\ L_\pm(k) &= \exp\left[\pm\frac{1}{2\pi \mathrm{i}}\int_{-\infty}^{\infty}\frac{\ln L(\xi)}{\xi - k}\,d\xi\right] \quad (\pm\Im k > 0). \end{aligned} \tag{29}$$

Equation (25) can be represented in the form

$$\begin{aligned} L_+(k) w_+(k) + \frac{M_2 w_-(k)}{M_1 L_-(k)} &= G(k)\left[\frac{M_1}{M_2}L_+(k) - \frac{1}{L_-(k)}\right], \\ G(k) &= \frac{M_2 C}{M_1(0+\mathrm{i}k)[1 - \varkappa_2/\varkappa_1 + (M_1 - M_2)(0+\mathrm{i}kv)^2]}. \end{aligned} \tag{30}$$

In particular, when $M_1 = M_2 = M$, we have

$$\begin{aligned} G(k)\left[L_+(k) - \frac{1}{L_-(k)}\right] &= C_1 + C_2, \\ C_1 = \frac{g}{\mathrm{i}k}[L_+(k) - L_+(0)], \qquad C_2 &= \frac{g}{0+\mathrm{i}k}\left[L_+(0) - \frac{1}{L_-(k)}\right]. \end{aligned} \tag{31}$$

The solution $w_\pm(k)$ of (30) has the form

$$w_+(k) = \frac{g}{\mathrm{i}k}\frac{L_+(k) - L_+(0)}{L_+(k)}, \qquad w_-(k) = \frac{g}{0+\mathrm{i}k}[L_+(0)L_-(k) - 1]. \tag{32}$$

In particular, using the limiting relations

$$w(\pm 0) = \lim_{k \to \pm\mathrm{i}\infty}(\mp\mathrm{i}k) w_\pm(k), \quad L_\pm(\pm\mathrm{i}\infty) = 1 \tag{33}$$

we find that

$$w(+0) = w(-0) = w(0) = g[L_+(0) - 1] \tag{34}$$

with

$$L_+(0) = \sqrt{\frac{\varkappa_1}{\varkappa_2}}\exp\left[\frac{1}{\pi}\int_0^\infty \frac{\operatorname{Arg} L(k)}{k}\,dk\right], \tag{35}$$

where $\operatorname{Arg} L(k)$ is equal to zero in a vicinity of $k = 0$ and exponentially decreasing as $k \to \infty$.

https://doi.org/10.1112/S0025579314000321 Published online by Cambridge University Press

§5. *Transition wave in the model of a failing bridge.* The averaging procedure can be applied in the regime when the wavelength corresponding to flexural vibrations of the bridge is sufficiently large compared to the distance between the supporting pillars. The homogenized model incorporates the fourth-order partial differential equation

$$D\frac{\partial^4 w(x,t)}{\partial x^4} + m\frac{\partial^2 w(x,t)}{\partial t^2} + \varkappa w(x,t) = mg, \tag{36}$$

where $w$ is the transverse displacement generated by flexural vibrations, $\varkappa$ is the foundation stiffness and $g$ is the acceleration of gravity.

In particular, in the steady-state regime, the solution depends only on $\eta = x - vt$, where $v$ is the failure wave speed. The equation of motion (36) becomes

$$Dw(\eta)^{IV} + mv^2 w''(\eta) + \varkappa\, w(\eta) = mg, \tag{37}$$

with $\varkappa = \varkappa_1$, when $\eta > 0$, and $\varkappa = \varkappa_2 < \varkappa_1$, when $\eta < 0$. Additional radiation conditions are imposed at infinity to complete the formulation, as in [**4**].

We use the same normalization of the spatial and time-like variables as in §3.1. Also we use a similar decomposition of the solution as in (14). The above problem allows for a closed form analytical solution, and the normalized dynamic displacement at the point $\eta = 0$, representing the front of the transition wave, is

$$w(0) = \begin{cases} \left(\sqrt{\dfrac{\varkappa_1}{\varkappa_2}} - 1\right)g, & 0 \leqslant v < v_2 = \sqrt{2}(\hat{\varkappa})^{1/4}, \\ \dfrac{v^2 - 2\hat{\varkappa} - \sqrt{v^4 - 4\hat{\varkappa}}}{2\hat{\varkappa}}g, & v_2 < v < v_1 = \sqrt{2}, \\ -\dfrac{v^2 - \sqrt{v^4 - 4\hat{\varkappa}}}{\sqrt{v^4 - 4} + \sqrt{v^4 - 4\hat{\varkappa}}}\dfrac{1 - \hat{\varkappa}}{\hat{\varkappa}}g, & v > v_1. \end{cases} \tag{38}$$

The graph of $w(0)$ versus $v$ is shown in Figure 4.

In physical models of gravity-driven transition waves, the steady-state regime is linked to configurations where $w(0) > 0$, and an increase in velocity leads to a decrease in the energy release rate or a decrease in the displacement at the front of the transition wave. Hence, this instantly identifies the interval for the values of speed of the transition wave, also shown by a shadowed rectangle in Figure 4:

$$\sqrt{2}\hat{\varkappa}^{1/4} < v < \sqrt{1 + \hat{\varkappa}}. \tag{39}$$

This solution has been applied to a practical analysis of the failure of San Saba bridge in Texas. The long San Saba railway bridge (Figure 3(b)) in central Texas (also known as Harmony Ridge Bridge, 3114′07″ N, 9833′52″ W) collapsed in May 2013 as a result of initial damage caused by fire. A 300-yard bridge fell apart after catching fire in a dramatic collapse. This event was the subject of media attention worldwide. A gravity driven transition wave was observed and

https://doi.org/10.1112/S0025579314000321 Published online by Cambridge University Press

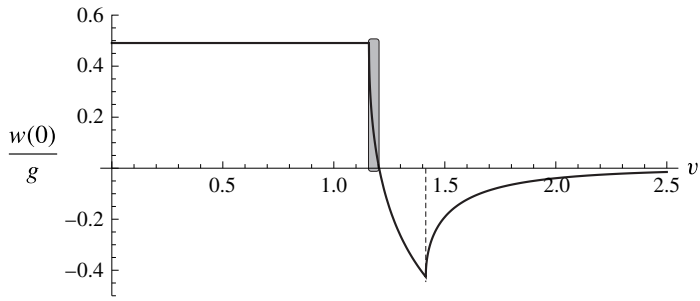



Figure 4: Displacement at the transition point as a function of velocity for the stiffness ratio $\varkappa = 0.45$. The shadowed rectangle indicates the possible steady-state region for the propagating fault.

recorded. According to the measurements taken, this wave reached the steady state in the final stages of the collapse of the bridge. An approximation of the wave speed, as offered by the asymptotic model, is

$$V = \left(\frac{D\kappa}{\rho^2 A^2}\right)^{1/4} = 24.3 \quad [\text{m sec}^{-1}] \tag{40}$$

where $D$, $\rho$ are the flexural rigidity and the linear mass density of the bridge, respectively, and $\kappa$ is the stiffness of the supporting pillars. Incidentally, the experimental measurement gives the value of 22.4 [m sec$^{-1}$]. The analytical model presented here explains the nature of the transition wave, shows that such a wave has a steady-state regime, and provides an accurate estimate for the speed of steady-state propagation of the failure wave.

§6. *Continuous versus discrete solution.* In the case of massless flexural links connecting the junction points, the stiffness coefficients will be the same as in the static case, i.e. as $v \to 0$, taking the form

$$\begin{aligned} \mathcal{V}^0_{w0} = \mathcal{V}^0_{wa} = \frac{12}{a^3}, \qquad & \mathcal{V}^0_{\phi 0} = \mathcal{V}^0_{\phi a} = -\frac{6}{a^2}, \\ \mathcal{M}^0_{w0} = -\mathcal{M}^0_{wa} = \frac{6}{a^2}, \qquad & \mathcal{M}^0_{\phi a} = -2\mathcal{M}^0_{\phi 0} = \frac{4}{a}, \end{aligned} \tag{41}$$

where the superscript $^0$ is used to denote the limit static values.

Two models referring to the discrete and the continuous systems have been highlighted here. The comparison of the values of the flexural displacement $w(0)$ obtained in these models is presented in Figure 5. The approaches indicate the same transition region, where the displacement $w(0)$ is a monotonically decreasing function of the speed of the propagating fault. We also note that in [**11**] and in [**9**] similar computations were produced for evaluation of the energy release rate at the vertex of a crack propagating through a lattice.

Both models contribute to the important explanation of the failure wave observed during the collapse of the San Saba bridge. For the discrete system

https://doi.org/10.1112/S0025579314000321 Published online by Cambridge University Press

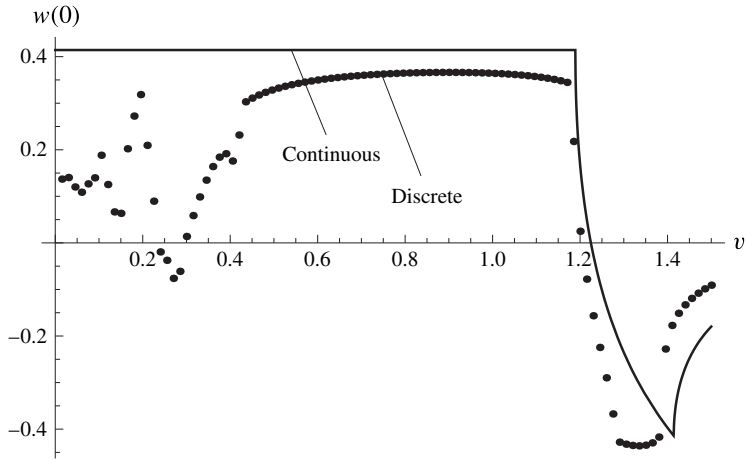



Figure 5: Flexural displacement $w(0)$ at the transition point as a function of the speed steady-state velocity $v$. The continuous model is compared with the discrete massless beam model. Results are given for $\varkappa_2/\varkappa_1 = 0.5$ and $a = 2$.

the pass bands (see Figure 5) are identified for flexural waves corresponding to the vibrations leading to the collapse. This also gives the required range of frequencies. Following that, the continuous model enables one to derive a simplified explicit solution, which produces $w(0)$ in closed analytical form. Both predictions agree well with the experimental observation, as also shown in Figure 5.

*Acknowledgements.* G.F.G. and M.B. wish to acknowledge the financial support of the Regione Autonoma della Sardegna (LR7 2010, grant "M4" CRP-27585). M.B. and A.B.M. acknowledge the financial support of the European Community's Seven Framework Programme under contract numbers PIEF-GA-2011-302357-DYNAMETA.

## *References*

1. M. Brun, G. F. Giaccu, A. B. Movchan and N. V. Movchan, Asymptotics of eigenfrequencies in the dynamic response of elongated multi-structures. *Proc. R. Soc. Lond. Ser.* A **468** (2012), 378–394, doi:10.1098/rspa.2011.0415.
2. M. Brun, A. B. Movchan and I. S. Jones, Phononic band gap systems in structural mechanics: finite slender elastic structures and infinite periodic waveguides. *J. Vib. Acous.* **135**(4) (2013), 041013, doi:10.1115/1.4023819.
3. M. Brun, A. B. Movchan, I. S. Jones and R. C. McPhedran, Bypassing shake, rattle and roll. *Phys. World* **26**(5) (2013), 32–36.
4. M. Brun, A. B. Movchan and L. I. Slepyan, Transition wave in a supported heavy beam. *J. Mech. Phys. Solids* **61**(10) (2013), 2067–2085, doi:10.1016/j.jmps.2013.05.004.
5. P. G. Ciarlet, *Plates and Junctions in Elastic Multi-Structures: An Asymptotic Analysis*, Masson and Springer (Paris and Heidelberg, 1990).
6. P. G. Ciarlet, *Mathematical Elasticity, Vol. II: Theory of Plates* (*Studies in Mathematics and its Applications*), North-Holland (Amsterdam, 1997).
7. V. A. Kozlov, V. G. Maz'ya and A. B. Movchan, *Asymptotic Analysis of Fields in Multi-Structures*, Oxford University Press (Oxford, 1999).

https://doi.org/10.1112/S0025579314000321 Published online by Cambridge University Press

**8.** H. Le Dret, *Problèmes Variationnels dans les Multi-domaines: Modèlisation des Jonctions et Applications*, Masson (Paris, 1991).
**9.** G. S. Mishuris, A. B. Movchan and L. I. Slepyan, Localised knife waves in a structured interface. *J. Mech. Phys. Solids* **57**(12) (2009), 1958–1979, doi:10.1016/j.jmps.2009.08.004.
**10.** G. P. Panasenko, *Multi-Scale Modelling for Structures and Composites*, Springer (Dordrecht, 2005), doi:10.1007/1-4020-2982-9.
**11.** L. I. Slepyan, *Models and Phenomena in Fracture Mechanics*, Springer (Berlin, 2002).

Alexander B. Movchan,
Department of Mathematical Sciences,
University of Liverpool,
Liverpool, L69 7ZL,
U.K.
E-mail: abm@liv.ac.uk

Michele Brun,
Department of Mathematical Sciences,
University of Liverpool,
Liverpool, L69 7ZL,
U.K.
and
Dipartimento di Ingegneria Meccanica,
Chimica e dei Materiali,
Universitá di Cagliari,
Piazza d'Armi, I-09123 Cagliari,
Italy
E-mail: mbrun@unica.it

Leonid I. Slepyan,
School of Mechanical Engineering,
Tel Aviv University,
PO Box 39040,
Ramat Aviv 69978 Tel Aviv,
Israel
E-mail: leonid@eng.tau.ac.il

Gian F. Giaccu,
Dipartimento di Ingegneria Meccanica,
Chimica e dei Materiali,
Universitá di Cagliari,
Piazza d'Armi, I-09123 Cagliari,
Italy
and
Department of Architecture,
Design and Urban Planning,
University of Sassari,
Piazza Duomo 6, Alghero,
Italy
E-mail: gf.giaccu@uniss.it

https://doi.org/10.1112/S0025579314000321 Published online by Cambridge University Press